

## Helium transport investigations at ASDEX Upgrade

A. Kappatou<sup>1,2</sup>, R.M. McDermott<sup>1</sup>, C. Angioni<sup>1</sup>, T. Pütterich<sup>1</sup>, R. Dux<sup>1</sup>, R.J.E. Jaspers<sup>3</sup>, E. Viezzer<sup>1</sup>, M. Cavedon<sup>1,4</sup>, R. Fischer<sup>1</sup>, M. Willensdorfer<sup>1</sup>, G. Tardini<sup>1</sup>, the EUROfusion MST1 Team\* and the ASDEX Upgrade Team

<sup>1</sup>Max-Planck-Institut für Plasmaphysik, Garching, Germany

<sup>2</sup>FOM Institute DIFFER, Eindhoven, The Netherlands

<sup>3</sup>Technische Universiteit Eindhoven, Eindhoven, The Netherlands

<sup>4</sup>Technische Universität München, Garching, Germany

### Introduction

Understanding low-Z impurity transport in fusion plasmas, particularly helium transport, is critical for the successful operation of future fusion reactors. Experimentally validated theoretical tools for the description of the transport mechanisms which define the shape of the helium density profile are necessary. In this way, predictions can be made and the extent of the accumulation of helium “ash” in the plasma core, leading to dilution of the fusion fuel, can be evaluated. To this end, helium transport investigations have been undertaken at ASDEX Upgrade (AUG) by means of charge exchange spectroscopy and quasi-linear gyrokinetic simulations.

### Forward modelling of the helium plume emission

To evaluate the helium CX spectra correctly and obtain accurate helium density profiles, forward modelling of the helium plume emission is necessary [1]. The existence of the helium plume emission in the CX spectra measured at AUG has been identified through an apparent discrepancy between the  $T_i$  and  $v_\phi$  profiles obtained from  $\text{He}^{2+}$  and  $\text{B}^{5+}$  and through an apparent discrepancy between the  $\text{He}^{2+}$  density profiles measured with different diagnostic geometries.

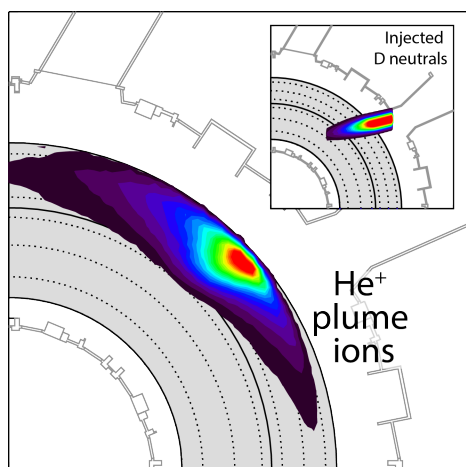


Figure 1: *Spatial distribution of helium plume ions.*

A model to describe the plume emission has been developed at AUG [2]. First, the density of the helium plume ions ( $\text{He}^+$ ) that are born in the beam volume from charge exchange reactions between fully stripped helium ions and the beam neutrals is calculated. Then, the spatial distribution of these ions along the magnetic field lines (see Fig. 1) is evaluated in a full 3D geometry, taking into account the magnetic equilibrium and the geometries of the neutral beam and the diagnostic. Transport perpendicular to the magnetic field lines is negligible within the lifetime of a  $\text{He}^+$  ion and is, therefore, neglected. Subsequently, some of the  $\text{He}^+$  ions undergo electron impact

excitation in the lines-of-sight of the diagnostic, and the associated plume photon flux is derived using the appropriate photon emission coefficients.

The accurate description of the plume ion distribution in real and velocity space requires non-Maxwellian effects to be taken into account. The plume particles are not quickly equilibrated

\* See <http://www.euro-fusionscipub.org/mst1>.

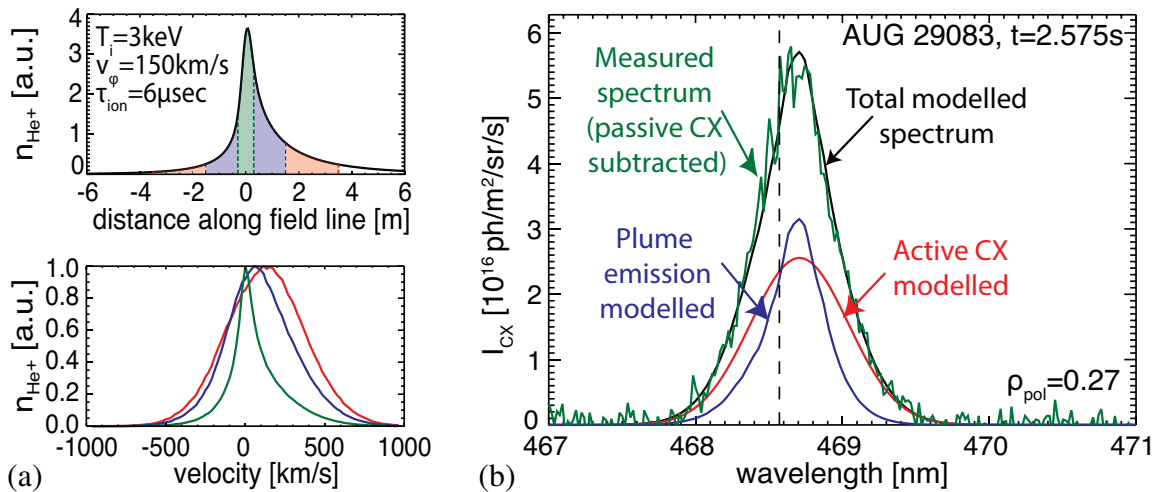


Figure 2: a) Distribution of plume ions along a field line (which intersects the neutral beam at 0 m) and the corresponding velocity distributions, summed over the ranges indicated. b) Reconstruction of a helium CX spectrum (the passive emission is subtracted applying neutral beam modulation). The sum of the modelled plume and prompt emissions agrees well with the measured spectra.

with the background ions, as the momentum exchange time is much larger than the ionisation time. As a result, the faster particles of the initial Maxwellian distribution leave the observation volume, while the slower ones remain, leading to apparent lower ion temperatures and rotation values in the observed plume emission.

This effect is illustrated in Fig. 2a, where the distribution of  $\text{He}^+$  ions along a magnetic field line is shown for typical core plasma parameters. Assuming lines-of-sight tangential to the field lines and no magnetic field line curvature, all of the particles will be observed. For instance, if all particles along the field line are summed together ( $\sim 7\text{ m}$ , red shaded region), then the velocity distribution is almost Gaussian (bottom plot, red line). In reality, however, the sum is over a much narrower range ( $\sim 60\text{ cm}$ , green shaded region), resulting in a much narrower velocity distribution and thus a “colder” and “slower” emission line (green line). In order to deal with this situation, a Monte Carlo approach is used to describe the distribution of the plume ions along the magnetic field lines. The Monte Carlo modelling provides the spread of the plume ions and their velocities, thus enabling the non-Maxwellian features to be accurately described.

The developed plume emission model reproduces the experimental CX spectra, as shown in Fig. 2b. The sum of the reconstructed active CX and plume emission lines are shown to agree well with the measured spectrum, from which the passive emission line is subtracted by means of neutral beam modulation. It is, therefore, concluded that the underlying physics mechanisms are adequately described. Furthermore, the  $T_i$  and  $v_\phi$  profiles obtained from the measured spectra, once the plume emission line is subtracted, agree within errorbars with those obtained from  $\text{B}^{5+}$  measurements.

### Experimental database for the investigation of helium transport

The high quality spectroscopic data and the plume correction enable detailed helium transport studies to be performed at AUG [2]. A database of 131 helium and boron density profiles was

assembled from dedicated experiments ( $I_p = 600\text{ kA}$ ,  $B_t = -2.5\text{ T}$ ). Different levels of central electron cyclotron resonance heating (ECRH) were applied ( $P_{\text{ECRH}} = 0 - 4\text{ MW}$ ) to vary the normalised gradient of the electron density ( $R/L_{n_e} = -(R/n_e)(dn_e/dr) = 0.03 - 3.6$ ) and of the toroidal rotation profiles ( $u' = -0.15 - 1.1$ ). Strong peaking of the electron density profile is known to occur with the application of central ECRH if the plasma turbulence regime transitions from ITG towards TEM [3]. At the same time, flat or even hollow rotation profiles have been observed [4]. Different levels of neutral beam heating ( $P_{\text{NBI}} = 2.5 - 7.5\text{ MW}$ ) as well as on- and off-axis beams were used to scan the ion temperature gradient ( $R/L_{T_i} = 3.0 - 7.0$ ) and Mach number. The effective collisionality is  $\nu_{\text{eff}} = \nu_{ei}/(c_s/R) = 0.3 - 1.9$  (all values for  $\rho_{\text{tor}} = 0.5$ ).

Both helium and boron, the dominant low-Z impurities after boronisation at AUG ( $c_B = 0.3 - 0.8\%$ ,  $c_{\text{He}} = 0.5 - 1.5\%$ ), were measured simultaneously, allowing a multi-species study. A wide variety of experimental helium and boron density profiles were obtained, with helium density profiles varying from almost flat to peaked ( $R/L_{n_{\text{He}}} = -0.1 - 4$ ) and boron density profiles varying from slightly hollow to peaked ( $R/L_{n_B} = -0.4 - 2.3$ ). The peaking of the helium density profile is comparable to that of the electron density at mid-radius, consistent with results obtained in DIII-D [5].

### Comparison of experimental results to the predictions of gyrokinetic modelling

The assembled database enables comparison of the experiment with gyrokinetic simulations over a wide parameter range. Neoclassical transport, calculated with NEOART [6], was confirmed to be negligible around mid-radius in comparison to the turbulent transport. Local quasi-linear gyrokinetic simulations of the turbulent transport have been performed with GKW [7]. The simulations are performed over a spectrum of  $k_y\rho = 0.23 - 0.75$ , providing the diagonal and off-diagonal contributions of impurity transport: the predicted impurity density density gradients are the sum of thermodiffusive, rotodiffusive and pure convection terms. Previous work at AUG showed that the logarithmic boron density gradients can be qualitatively [3] and even quantitatively [8] reproduced, provided that “roto-diffusion” is included.

The experimentally deduced  $R/L_{n_{\text{He}}}$  and  $R/L_{n_B}$  are compared with the gyrokinetic modelling predictions in Fig. 3a for a subset of the database, corresponding to discharges 30367 and 30368, plotted for illustration against  $R/L_{n_e}$ . The centrally applied ECRH power was scanned up to a maximum of 4MW on a background of 2.5MW of NBI heating. Clear differences are

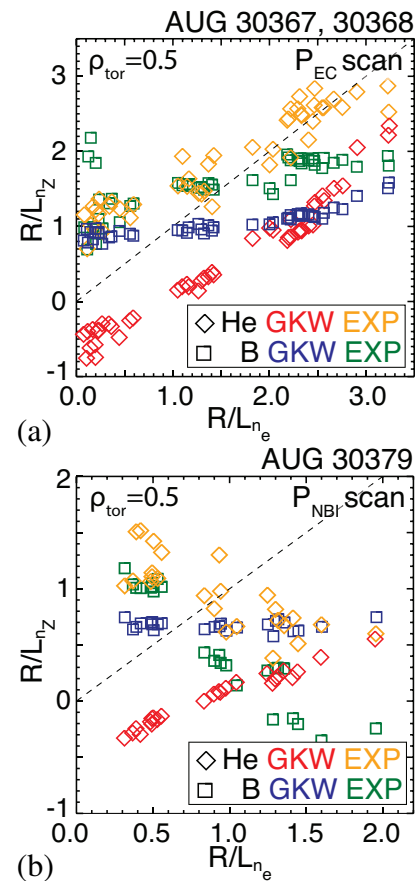


Figure 3:  $R/L_{n_{\text{He}}}$  and  $R/L_{n_B}$  from gyrokinetic modelling and experimental measurements, plotted against  $R/L_{n_e}$ .

observed between helium and boron, a behaviour predicted theoretically, as thermodiffusion is more important for lower-Z impurities, due to the inverse charge dependence of the thermodiffusive term. Only a qualitative agreement for both impurities is reproduced, as the theory underpredicts the experimental gradients, in contrast to previous results.

However, cases also exist in the database in which opposite trends are observed. In discharge 30379, a scan of NBI power was performed on a background of 0.5 MW of ECRH power. The experimental gradients of both helium and boron are found to decrease with increasing  $R/L_{n_e}$  (shown in Fig. 3b), as well as with increasing  $R/L_{T_i}$  and  $u'$  (not shown). This behaviour is not reproduced by the gyrokinetic simulations.

An explicit explanation for the observed features is not straightforward. In the discharges in the database, strong sawteeth or MHD modes were not identified. The effect of ELMs on the profiles is minimised by selecting inter-ELM profiles. The sensitivity of the gyrokinetic modelling to the used magnetic equilibrium [8] was tested, but the uncertainties in the magnetic equilibrium are not big enough to explain the observations. The effect of a helium source at the tokamak wall on the helium density profile gradient was assessed with STRAHL [9] and was found to be too small to explain the discrepancies between the experiment and theory. And examining each turbulent transport term that contributes to the impurity density gradients, obtained from the gyrokinetic modelling, does not lead to a direct conclusion on which term is responsible for the discrepancy. Disentangling the dependencies of the impurity density gradients on the different plasma parameters in order to address these discrepancies is the aim of further experimental and modelling work.

## Conclusions

Investigations of light impurity transport have been performed at ASDEX Upgrade including, for the first time, accurate helium measurements, supported by the plume emission modelling. The shape of the helium density profile is found experimentally to follow closely the shape of the electron density profile. The current theoretical understanding of light impurity transport, as derived from quasi-linear gyrokinetic simulations, is compared against the experiment, revealing some troubling discrepancies. As the impurity density profiles are defined by the interplay of many plasma parameters, further work from both the theoretical and the experimental side are needed in order to decorrelate the parameters that define low-Z impurity transport.

## References

- [1] R.J. Fonck *et al*, Phys. Rev. A **29**, 3288 (1984)
- [2] A. Kappatou, PhD thesis, Eindhoven University of Technology, the Netherlands (2014)
- [3] C. Angioni *et al*, Nucl. Fusion **51**, 023006 (2011)
- [4] R.M. McDermott *et al*, Plasma Phys. Control. Fusion **53**, 035007 (2011)
- [5] D.F. Finkenthal, PhD thesis, University of California, Berkeley (1994)
- [6] R. Dux and A.G. Peeters, Nucl. Fusion **40**, 1722 (2000)
- [7] A.G. Peeters *et al*, Comput. Phys. Commun. **180**, 2650 (2009)
- [8] F.J. Casson *et al*, Nucl. Fusion **53**, 063026 (2013)
- [9] R. Dux, STRAHL, Annual IPP report **10/30** (2006)